


Article

A Remote Sensing Water Information Extraction Method Based on Unsupervised Form Using Probability Function to Describe the Frequency Histogram of NDWI: A Case Study of Qinghai Lake in China

Shiqi Liu ¹, Jun Qiu ^{1,2,*} and Fangfang Li ³ 

¹ School of Civil Engineering and Water Resources, Qinghai University, Xining 810016, China; ys220859020445@qhu.edu.cn

² Department of Water Resources and Hydropower Engineering, Tsinghua University, Beijing 100084, China

³ School of Water Resources and Civil Engineering, China Agricultural University, Beijing 100091, China; liff@cau.edu.cn

* Correspondence: aeroengine@tsinghua.edu.cn

Abstract: With escalating human activities and the substantial emissions of greenhouse gases, global warming intensifies. This phenomenon has led to increased occurrences of various extreme hydrological events, precipitating significant changes in lakes and rivers across the Qinghai Tibet Plateau. Therefore, accurate information extraction about and delineation of water bodies are crucial for lake monitoring. This paper proposes a methodology based on the Normalized Difference Water Index (NDWI) and Gumbel distribution to determine optimal segmentation thresholds. Focusing on Qinghai Lake, this study utilizes multispectral characteristics from the US Landsat satellite for analysis. Comparative assessments with seven alternative methods are conducted to evaluate accuracy. Employing the proposed approach, information about water bodies in Qinghai Lake is extracted over 38 years, from 1986 to 2023, revealing trends in area variation. Analysis indicates a rising trend in Qinghai Lake's area following a turning point in 2004. To investigate this phenomenon, Pearson correlation analysis of temperature and precipitation over the past 38 years is used and unveils the fact that slight precipitation impacts on area and that there is a positive correlation between temperature and area. In conclusion, this study employs remote sensing data and statistical analysis to comprehensively investigate mechanisms driving changes in Qinghai Lake's water surface area, providing insights into ecological shifts in lake systems against the backdrop of global warming, thereby offering valuable references for understanding and addressing these changes.

Keywords: remote sensing; NDWI; water body



Citation: Liu, S.; Qiu, J.; Li, F. A Remote Sensing Water Information Extraction Method Based on Unsupervised Form Using Probability Function to Describe the Frequency Histogram of NDWI: A Case Study of Qinghai Lake in China. *Water* **2024**, *16*, 1755. <https://doi.org/10.3390/w16121755>

Academic Editors: Cesar Andrade and Hucai Zhang

Received: 23 March 2024

Revised: 15 June 2024

Accepted: 18 June 2024

Published: 20 June 2024



Copyright: © 2024 by the authors. Licensee MDPI, Basel, Switzerland. This article is an open access article distributed under the terms and conditions of the Creative Commons Attribution (CC BY) license (<https://creativecommons.org/licenses/by/4.0/>).

1. Introduction

With the intensification of human activities and the massive emission of greenhouse gases, climate warming is occurring. The warming rate of the Qinghai Tibet Plateau, known as the “Asian Water Tower”, is 0.36 °C/10a [1], which is about twice the global warming rate [2].

The lakes and rivers on the Qinghai Tibet Plateau have undergone significant changes. Remote sensing technology has been applied in recent years to accurately isolate and extract information about water bodies due to its wide monitoring range, fast acquisition, relatively short imaging period, and ability to collect large amounts of information. Furthermore, the process of collecting remote sensing data is not subject to the subjective influences of human factors, thereby ensuring higher objectivity and consistency in the data, and consequently providing more reliable water body information.

As a commonly employed method for remote sensing water information extraction, the water index approach possesses distinctive advantages but also entails limitations. Leveraging the reflective properties of ground objects across various spectral bands, it

accentuates and enhances target entities. By integrating operations across multiple spectral bands, it constructs a water index, facilitating the rapid and precise extraction of water-related information. Moreover, the extraction of information about water boundary ranges is comparatively precise. Nevertheless, the coexistence of phenomena such as “same-spectrum, different objects” and “different-spectrum, same objects” leads to challenges like misclassification and leakage. Consequently, determining the optimal threshold for the water index method typically necessitates adjustments and optimizations through experimentation and practical application [3].

Liu et al. used 10 water index methods to extract information about water bodies from Landsat and Sentinel-2 images in Jilin Province, China. The Otsu algorithm was used to adaptively determine the segmentation threshold for each indicator, and the indicators were compared in terms of inter-class separability, threshold sensitivity, optimal threshold robustness, and water information extraction accuracy [4].

Currently, researchers have extensively investigated water body detection across various contexts, leveraging water indices, multispectral data sources, and spatial resolution, in an endeavor to devise methodologies addressing this issue. Presently, emphasis lies on two pivotal stages within the application framework of this approach. Firstly, the development and selection of water indices under diverse circumstances are undertaken, succeeded by the determination of an optimal segmentation threshold [3]. This study is confined solely to the determination of the optimal segmentation threshold for the NDWI (Normalized Difference Water Index) [5].

Global thresholding methods [6] encompass Otsu’s method, which maximizes inter-class variance [7], the minimum error method [8], and the maximum entropy method [9]. The minimum error method operates on the assumption of a proportional relationship between misclassification probabilities of background and target objects. The optimal segmentation threshold, corresponding to minimizing misclassification, achieves image segmentation. The fundamental principle of the maximum entropy method is to identify the threshold that maximizes the sum of Shannon entropy for two regions, thereby determining the optimal segmentation threshold. The advantage of global thresholding methods lies in their straightforward principles and ease of implementation. However, they may encounter challenges in determinacy and susceptibility to local optima. In images with significant noise, segmentation outcomes may prove unsatisfactory.

Machine learning algorithms are extensively utilized in image segmentation due to their ability to effectively leverage complex image features; handle nonlinear relationships; exhibit flexibility and generalization capabilities; facilitate automated image segmentation processes such as maximum likelihood; and Support Vector Machines [10], decision trees [11], random forests, K-means [12], etc. With the decision tree method, optimal features of the data are identified through several judgment conditions, gradually refining them into two parts. In remote sensing image extraction, it is often combined with single-band and exponential methods, offering rapid computation. However, decision trees are highly sensitive to minor variations in input data, which may result in different trees being generated on different training datasets, thereby lacking stability. Random forests necessitate the construction of multiple decision trees, each considering randomly selected features at each node, akin to a “voting system,” undoubtedly increasing computational costs, particularly on large-scale datasets.

The emergence and development of deep learning are due to the advancement of big data, computing resources, and algorithm theory. A large amount of data can provide rich training samples for training deep neural networks; high performance computing resources can support large-scale parameter training and complex network structures; and the continuous advancement of algorithm theory provides more effective optimization algorithms and training techniques, enabling deep neural networks to learn and generalize better [13].

The Fully Convolutional Network (FCN) proposed by Long et al. [14]. in 2015 is a pioneering work in the field of deep learning for semantic segmentation [15]. It can support images of any size as input. FCN replaces the fully connected layer behind the traditional Convolutional Neural Networks (CNN) with a convolutional layer, so that the network’s

output will be a heatmap rather than a category. At the same time, to address the issue of image size reduction caused by convolution and pooling operations, the upsampling Up Sample method is used to restore image size. To a certain extent, it has promoted the development of semantic segmentation, but the drawbacks are also obvious. The upsampling operation is rough, and the loss of details is also very serious, ignoring the connection between pixels [16].

In 2015, Olaf Ronneberger et al. proposed U-Net [17], which is based on a symmetric encoder decoder structure. In order to reduce the loss of detail information caused by convolutional pooling operations, this network uses skip connections to compensate for lost information for upsampling [18]. However, continuous upsampling cannot fully recover the loss of image detail information caused by max pooling, and the accuracy is limited.

In 2016, the International Conference on Learning Representation (ICLR) proposed atrous convolution, which is a convolutional approach proposed to address the loss of detail information by increasing the spacing between convolutional kernel elements to expand the receptive field [19].

The Deeplab [20–23] series is a semantic segmentation network developed by the Google team. The network combines dilated convolution to expand the receptive field, doubling the receptive field without increasing the number of parameters [21], and obtaining multi-scale feature information to improve segmentation accuracy.

Researchers found that increasing the number of layers in a network to a certain extent does not improve network performance, and could also lead to overfitting, vanishing gradients, or exploding gradients. Deep learning seemed to have entered a bottleneck. Therefore, in 2016, Kaiming He et al. proposed ResNet [24], also known as the Shortcut Connection by the author. In this network, residual blocks were first used. This design of the residual network makes the model easier to optimize, and even in networks with convolutional pooling depths exceeding 100 layers, performance can still be guaranteed, making it easier to find convergence points during the training process. At the same time, the drawbacks of ResNet are also obvious, requiring more computing resources for training and inference. Due to its depth and complexity, training may take a long time and the size of the model may also increase. Secondly, due to its large number of parameters, ResNet may overfit certain datasets. In practice, it may be necessary to use regularization techniques such as Dropout to alleviate overfitting problems [25].

In 2019, Ke Sun et al. proposed HRNet. It takes a high-resolution subnet as the first stage, gradually increasing the number of high-resolution to low resolution subnets to form more stages, and the subnets of multiple stages are connected in parallel through upsampling and convolution [26]. The network maintains high resolution throughout the entire process by continuously exchanging information and fusing multi-scale features. The resulting feature representations are not only strong, but also precise in space, which to some extent improves the problems of detail loss and insufficient accuracy in existing algorithms. However, a large amount of repeated fusion between multiple stages can also generate several times the computational complexity, and parameter quantity and dense feature fusion can also calculate a large amount of redundancy and the same information [16].

Due to the threshold determination in the water body index method for extracting information about water, it requires repetitive experimentation and visual judgment, which is empirical and highly subjective.

This paper proposes a method that utilizes input samples on NDWI imagery to infer the parameters μ and σ of the Gumbel distribution, thereby determining the optimal segmentation threshold T . The Gumbel distribution is widely employed in various fields such as oceanography, hydrology, meteorology, etc., for computing extreme high (or low) water levels associated with different return periods. The annual maximum water level can be regarded as being influenced by precipitation and numerous stochastic factors [27]. Based on the Normalized Difference Water Index (NDWI) [5], this study compares the accuracy of the proposed method with Support Vector Machine (SVM) [10], Otsu's method [7], K-means clustering [12], genetic algorithm (GA) [28], maximum likelihood estimation

(MLE), and AdaBoost [29]. Pixel-level fusion is employed to stitch and merge images, and, subsequently, information about the water surface area of Qinghai Lake from 1986 to 2023 is extracted and analyzed. The variation in Qinghai Lake's water surface area over 38 years is examined in correlation with trends in temperature, precipitation, and related factors.

2. Materials and Methods

2.1. Study Area

Qinghai Lake, located in the northeast of the Qinghai Tibet Plateau in China, is the largest inland lake and also the largest saltwater lake in China. It is an important water body that maintains ecological security in the northeast of the Qinghai Tibet Plateau [30]. Qinghai Lake is an important component of the Qinghai Tibet Plateau and plays a crucial role in maintaining local ecological balance. It provides habitat for a large number of aquatic organisms, including many rare and endangered species. Qinghai Lake also has a significant impact on the climate of the surrounding areas through water vapor evaporation, which helps to maintain and improve the regional ecological environment. Qinghai Lake is a natural climate and environmental monitoring station. By observing and studying Qinghai Lake, we can understand the environmental and climate change trends of the Qinghai Tibet Plateau and the world. This is of great significance for predicting and addressing climate change.

The Qinghai Lake Basin has abundant precipitation, and the high-altitude wetland ecosystems such as glaciers, rivers, swamps, and lakes play an irreplaceable role in regulating the climate, maintaining water conservation, and maintaining ecological balance in the northwest region. It is an important water source in the Yellow River Basin, an important water body for maintaining ecological security in the northeast of the Qinghai Tibet Plateau, and a natural ecological barrier for protecting the economic and social development of Qinghai Province in China.

Therefore, protecting Qinghai Lake is not only of great significance for maintaining local ecological, economic, and social sustainable development, but also of great value for global environmental protection and the future development of human society.

Qinghai Lake is located to the northwest of Xining City, Qinghai Province, China, between $99^{\circ}36'$ E and $100^{\circ}16'$ E, and between $36^{\circ}32'$ N and $37^{\circ}15'$ N. The lake is situated at an altitude of 3193.8 m above sea level, with a surface area of 4476 square kilometers, stretching 104 km from west to east and 62 km from north to south, as shown in Figure 1. It has an average water depth of 21 m, with a maximum depth of 27 m, and a water volume of 71.6×10^9 cubic meters. The drainage basin covers an area of 29,661 square kilometers (as of 2017) [30].

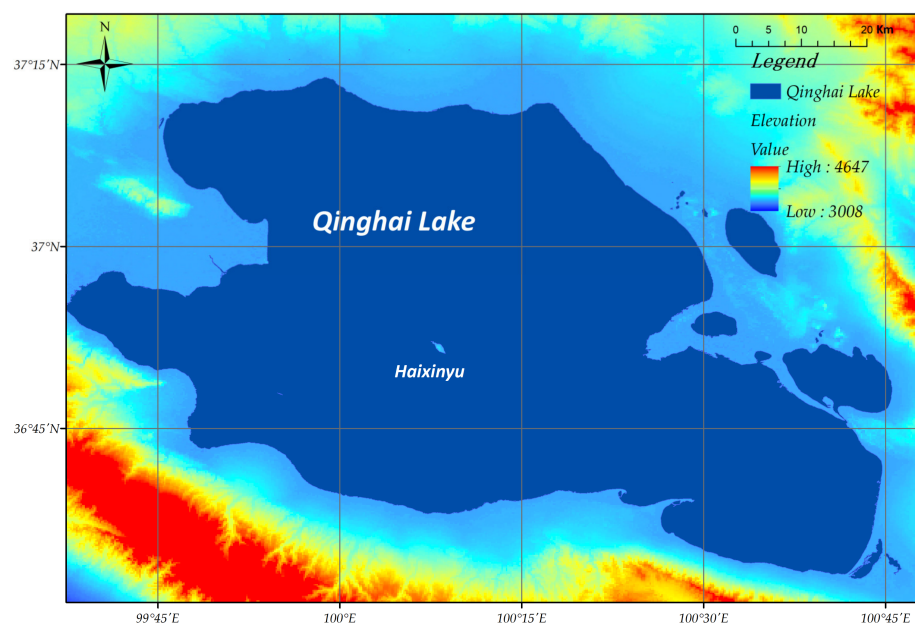


Figure 1. Qinghai Lake location information.

2.2. Data Processing

This study utilized data obtained from Landsat satellites, renowned for their rich spectral bands and moderate spatial resolution capabilities. Specifically, imagery from Landsat 9 captured on 21 March 2023, Landsat 8 captured on 15 October 2015, and Landsat 5 captured on 21 July 1998, were individually employed for analysis. Preliminary assessments confirmed the high quality of the selected imagery, free from atmospheric interferences such as cloud cover or fog. To ensure the accuracy and reliability of subsequent analyses, we conducted image cropping on the study area, resulting in a final cropped size of 3584×2304 pixels.

2.3. Methods

2.3.1. Calculating Multispectral Water Indices

The Normalized Difference Water Index (NDWI) is a widely utilized remote sensing technique employed to delineate water bodies and monitor water-related changes across various landscapes. NDWI quantifies the presence of water by exploiting the distinct absorption and reflection properties of water and non-water features in near-infrared (NIR) and green spectral bands. It is calculated as the normalized difference between the NIR and green bands, resulting in a numerical index that accentuates water bodies while suppressing background influences such as soil and vegetation. NDWI's robustness in discriminating water features amidst diverse environmental settings has rendered it invaluable in applications ranging from hydrological studies and ecosystem monitoring to agricultural management and urban planning. Its simplicity, efficiency, and effectiveness make NDWI a cornerstone in remote sensing-based water resource management and environmental assessment endeavors [31].

The Normalized Difference Water Index (NDWI) was proposed by McFeeters S K et al.; it maximizes the suppression of vegetation information and enhances water characteristics based on the different reflectance of water in the near-infrared and green light bands [5]. The following is the formula for water body index:

$$DWI = \frac{Green - NIR}{Green + NIR} \quad (1)$$

Green is the green band and *NIR*, Near Infrared, is the near-infrared band.

The histogram of the water index method roughly presents a bimodal shape, with an interval between $[-1, 1]$. The first peak is the frequency histogram of non-water bodies, while the second peak is water bodies. In theory, the optimal segmentation threshold is located at the lowest point between the two peaks, as shown in Figure 2. However, different seasons, months, and light conditions result in differences in the shape of histograms, and if there is cloud pollution, it may not exhibit bimodal characteristics. Here, we use the minimum frequency interval median between the two peaks as the optimal segmentation threshold.

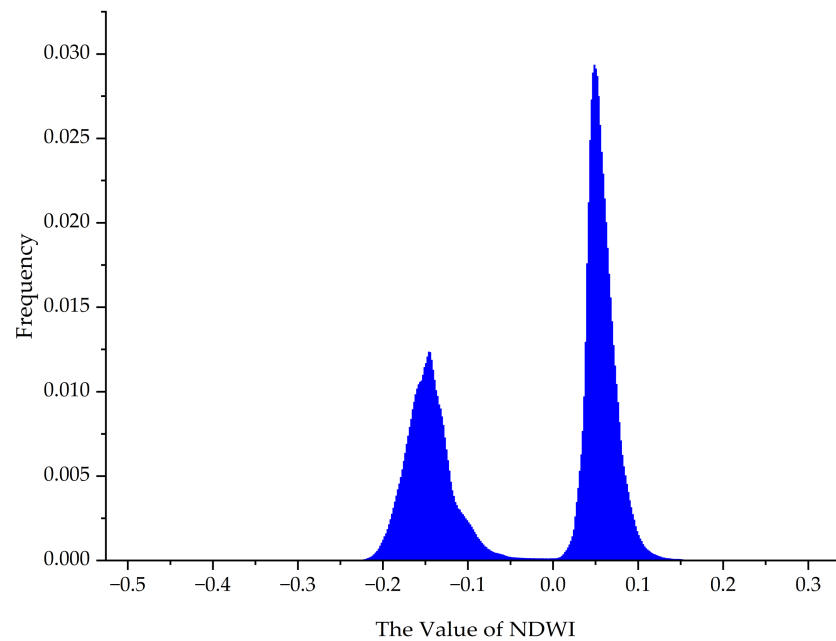


Figure 2. Frequency histogram of NDWI. The blue color in the figure represents the frequency histogram.

2.3.2. Machine Learning

NDWI-SVM (Support Vector Machine)

Support Vector Machine (SVM) was first proposed by Cortes and Vapnik [10], and is a supervised classification model commonly used in classification and regression analysis. The basic principle is to construct a hyperplane as the decision boundary by training the features of the samples, so that samples of different categories are distributed as widely as possible on both sides of the hyperplane. In remote sensing images, there are usually significant differences in the characteristics of water and non-water bodies, so SVM method can be used for water information extraction. The formula is as follows:

$$f(x) = \sum_{i=1}^n (\alpha_i - \alpha_i^*) K(x_i, x) + b \quad (2)$$

The kernel function used is the radial basis function.

$$K(x_i, x) = \exp(-g \|x_i - x\|^2) \quad (3)$$

$$0 \leq \alpha_i \leq C \quad (4)$$

where α_i and α_i^* are the Lagrange multipliers and $K(x_i, x)$ is the kernel function, which is the inner product of vectors x_i and x in the feature space.

Using the water pixel values and non-water pixel values of the training samples as input variables, the radial basis function is selected as the kernel function, and the model parameters, such as the penalty coefficient C and kernel function coefficient g , are adjusted to find the best model [32].

NDWI-K-Means

The K-means algorithm belongs to clustering algorithms and unsupervised classification. Its primary parameter is the number of clusters, denoted as K . Given the presence of two categories, water and non-water, the number of clusters is set to two. The cluster centers, representing the closest distances between the sample data and the centroids, are classified as the centroids. In this context, random points from the sample are used as initial cluster centers. The selection of centroids is determined using the Euclidean distance

method, with iterations continuing until the specified tolerance for error is met. This process is described by Equation (5).

$$d(x_i, x_j) = \|x_i - x_j\| = (x_i - x_j)^T (x_i - x_j) = \sqrt{\sum_{k=1}^n (x_{ik} - x_{jk})^2} \quad (5)$$

NDWI-MLE (Maximum Likelihood Estimation)

The maximum likelihood method is a statistical method used to estimate the probability distribution of data. In image segmentation, it can be used to determine the probability that a pixel point belongs to a particular category. It belongs to supervised classification, which takes water body and non-water body samples as input.

$$L(\theta) = \prod_{i=1}^n f(x_i; \theta) \quad (6)$$

$$\theta = \{\mu, \sigma\} \quad (7)$$

$$\ln L(\theta) = \sum_{i=1}^n \ln f(x_i; \theta) \quad (8)$$

$$\hat{\theta} = \operatorname{argmax}\{\ln L(\theta)\} \quad (9)$$

NDWI-AdaBoost

NDWI images are processed using the AdaBoost algorithm. Specifically, the weights are initialized, and then multiple rounds of iterations are performed with a weak classifier, updating the weights after each iteration until a preset number of iterations is reached or a preset error rate is reached [13]. The final water body extraction results are generated. The classification result of each pixel point is determined by the voting of the classification result of each weak classifier. The number of iterations is 100.

$$F(x) = \operatorname{sign}\left(\sum_{t=1}^T \alpha_t h_t(x)\right) \quad (10)$$

2.3.3. NDWI-Otsu

Otsu is an algorithm for determining the binarized segmentation threshold of an image; it was proposed by the Japanese scholar Otsu in 1979, and is regarded as the best method for global threshold selection in image segmentation.

$$\sigma^2 = \omega_0 (\mu_T - \mu_0)^2 + \omega_1 (\mu_T - \mu_1)^2 \quad (11)$$

$$T = \operatorname{argmax}\{\sigma^2\} \quad (12)$$

$$\mu_T = \omega_0 \mu_0 + \omega_1 \mu_1 \quad (13)$$

$$P_i = \frac{n_i}{M \times N} \quad (i = 0, 1, \dots, L - 1) \quad (14)$$

$$\omega_0 = \sum_{i=0}^T P_i \quad (15)$$

$$\omega_1 = \sum_{i=T+1}^{L-1} P_i = 1 - \omega_0 \quad (16)$$

$$\mu_0 = \sum_{i=0}^T \frac{i P_i}{\omega_0} \quad (17)$$

$$\mu_1 = \sum_{i=T+1}^{L-1} \frac{iP_i}{\omega_1} \quad (18)$$

2.3.4. NDWI-GA (Genetic Algorithm)

Genetic algorithm is an optimization search algorithm that draws on some phenomena in evolutionary biology, such as heredity, mutation, natural selection, and hybridization. By simulating the evolutionary process in nature, genetic algorithms are able to find the optimal solution in the search space, which is especially suitable for those problems that are difficult to solve directly by mathematical models. In image threshold segmentation, genetic algorithms can help to automatically find the optimal threshold value, thus, realizing image segmentation [28].

The parameters of the genetic algorithm are configured as follows: the chromosome length is set to 10, indicating the length of genetic encoding for each individual solution; a population size of 10 individuals is employed in each generation to constitute the evolving population; a crossover probability of 0.7 is applied, defining the likelihood of generating new individuals through crossover operation as 0.7; a mutation probability of 0.3 is utilized, denoting the probability of an individual undergoing mutation as 0.3 during the evolutionary process; and a maximum number of generations of 100 is specified, indicating the limit of iterations for the genetic algorithm, beyond which the algorithm terminates its execution.

2.3.5. NDWI-Gumbel

The manual method is intuitive but susceptible to subjective factors and is time-consuming. Maximum likelihood methods and automated determination methods based on expert systems, although relatively objective and accurate, are computationally intensive and require high levels of data and expert experience.

The Gumbel distribution has emerged as the preferred choice in extreme value analysis. This distribution possesses theoretical properties that render it particularly suitable for characterizing the distribution of extreme events. Moreover, its empirical fit to observed data in specific contexts often proves superior, further reinforcing the rationale for its application in extreme value analysis. Consequently, the selection of the Gumbel distribution as the foundational model for extreme value analysis is grounded in its theoretical advantages. Nonetheless, extensive testing of probability distributions has been conducted, yielding results that have not been entirely satisfactory.

In conclusion, determining the optimal threshold for NDWI is a complex process that requires the consideration of multiple factors and the use of scientific methods and tools for evaluation and optimization. In view of this, this paper proposes a water information extraction method based on Gumbel distribution classification.

It is assumed that both the water body and the background data frequency histogram must satisfy the Gumbel distribution.

First, the normalized water body index method is applied to the remote sensing image data. The pixel values of the NDWI images are taken as input. The Gumbel distribution parameters and mixture weights are estimated by great likelihood.

Where the formula of Gumbel distribution is as follows:

$$f(x|\mu, \sigma) = \frac{1}{\sigma} e^{-\frac{x-\mu}{\sigma}} - e^{-\frac{x-\mu}{\sigma}} \quad (19)$$

where μ is the position parameter and σ is the scale parameter.

Substitute the a priori samples into the probability density function by maximum likelihood estimation (MLE) to estimate the parameters μ and σ , respectively, as follows:

Then let the parameter set θ

$$f(x) = mf_1(x; \theta_1) + (1 - m)f_2(x; \theta_2) \quad (20)$$

where $\theta_1 = \{\mu_1, \sigma_1\}$ and $\theta_2 = \{\mu_2, \sigma_2\}$.

The parameters of the Gumbel distribution were estimated separately through the NDWI prior samples with the following equations:

$$L(\theta) = \prod_{i=1}^n f(x = x_i; \theta) \quad (21)$$

Both sides of the equation take logarithms:

$$\ln L(\theta) = \sum_{i=1}^n \ln f(x = x_i; \theta) \quad (22)$$

$$\hat{\theta} = \arg \max \ln L(\theta) \quad (23)$$

Derivation θ finally solves the parameter θ

$$\frac{d \ln L(\theta)}{d\theta} = 0 \quad (24)$$

Substitute the parameters θ and m into Equation (4) to obtain the mixed probability density function $f(x)$.

Then, the constructed probability density is derived to obtain the minimum value as follows:

$$x^* = \arg \min\{f(x)\} \quad (25)$$

$$\frac{df(x)}{dx} = 0 \quad (26)$$

The obtained solution serves as the optimal segmentation threshold used to distinguish water bodies from non-water bodies in the NDWI imagery.

The above figure shows the red curve as the mixed Gumbel distribution curve of water bodies and non-water bodies, as shown in Figure 3.

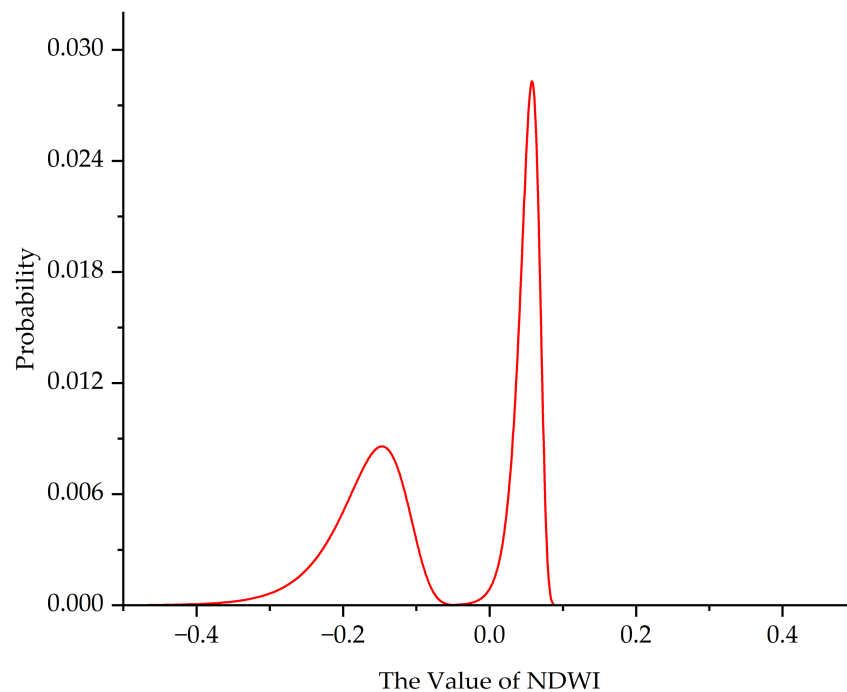


Figure 3. Mixed probability density distribution plot.

Next, the image elements of NDWI are individually discriminated one by one, and those larger than the threshold T are water bodies, and, conversely, those smaller than T

are non-water bodies. The segmented image $image_seg$ binarized image is obtained; 0 is non-water body and 1 is water body.

$$image_seg(i,j) = \begin{cases} 1, & NDWI(i,j) \geq T \\ 0, & NDWI(i,j) < T \end{cases} \quad (27)$$

3. Results

The following table shows the binary segmentation maps, number of pixels, and extraction area (km²) for the NDWI-Gumbel, NDWI, NDWI-SVM, NDWI-Otsu, NDWI-K-means, NDWI-GA, NDWI-MLE, and NDWI-AdaBoost methods, respectively (Table 1).

Table 1. Result.

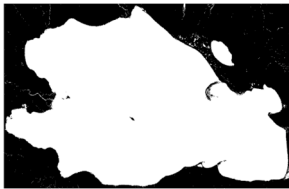


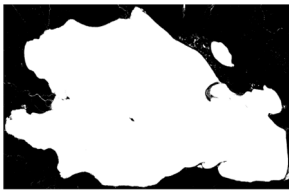




















Methods	2023/3/21-Landsat 9	2015/10/15-Landsat 8	1998/7/21-Landsat 5
NDWI-Gumbel			
NDWI			
NDWI-SVM			
NDWI-Otsu			
NDWI-Kmean			
NDWI-GA			

Table 1. Cont.

Methods	2023/3/21-Landsat 9	2015/10/15-Landsat 8	1998/7/21-Landsat 5
NDWI-MLE			
NDWI-AdaBoost			

Note: The red rectangular boxes in the segmentation image above represent water bodies that were mistakenly classified as non-water bodies, while the green rectangular boxes represent non-water bodies that were mistakenly classified as water bodies.

An accuracy evaluation of the binary categorization problem for water bodies and non-water bodies was made using a 2×2 confusion matrix with the horizontal coordinate as the true category, the vertical coordinate as the predicted category, and the number of pixels within the matrix.

Random sampling of 10,000 points: in a semantic segmentation task, firstly, the image needs to be randomly sampled and about 10,000 points are selected as samples. These points should cover all kinds of semantic regions in the image, including different objects, backgrounds and edges, etc. [33].

Visual discrimination: 20,000 randomly sampled points are annotated on each original image to visually discriminate the semantic category of each point. This step requires manual completion with the assistance of a semi-automatic annotation tool. Each sampled point needs to be accurately labeled with its corresponding semantic category.

Establishment of confusion matrix: the confusion matrix is a tool used to evaluate the performance of classification models. It provides insights into the accuracy and errors of the model across different classes. Specifically, for each semantic category i , the proportions of correct or incorrect classifications as i -class in the training samples are counted to construct a table. If the actual category is i and it is correctly classified as i , it is counted as true positive (TP); if the actual category is i but incorrectly classified as another category j ($j \neq i$), it is counted as false positive (FP); if the actual category is i but not covered by any predicted category i , it is counted as false negative (FN); if the actual category is i and correctly predicted as i , it is counted as true negative (TN). See Table 2.

Table 2. Confusion matrix.

		Real	
		Water	Other
Prediction	Water	True Positive	False Positive
	Other	False Negative	True Negative

Through the confusion matrix, the classification accuracy and error of the model when applied to each category can be visualized, so that the model can be optimized and adjusted. Meanwhile, the confusion matrix can also be used to guide data labeling and sample selection to improve the generalization ability of the model.

The evaluation indexes are total precision OA, precision rate precision, recall rate recall, Mean Intersection over Union (MIoU), as in Equations (26)–(29), respectively:

$$\text{Overall Accuracy} = \frac{TP + TN}{TP + TN + FP + FN} \times 100\% \quad (28)$$

$$\text{Precision} = \frac{TP}{TP + FP} \quad (29)$$

$$\text{Recall} = \frac{TP}{TP + FN} \quad (30)$$

$$\text{MIoU} = \frac{1}{k+1} \sum_{i=1}^k \frac{TP}{TP + FN + FP} \quad (31)$$

1. *Overall accuracy (OA)* is the most commonly used evaluation metric in image segmentation, and indicates the proportion of total pixels that are correctly classified by the segmentation algorithm. Overall accuracy gives a measure of the overall performance of the algorithm.
2. *Precision* is the probability that among all the pixels that are classified as positive examples, they are actually positive examples. It focuses on the prediction accuracy of the classifier for positive cases, i.e., whether the target region in the image is correctly recognized.
3. *Recall* is the probability that among all the pixels that are actually positive examples, they are correctly recognized as positive examples. It is concerned with the degree of coverage of the classifier with respect to the target region, i.e., whether all the target regions in the image are recognized.
4. *Mean Intersection over Union (MIoU)* is a more applicable evaluation metric for multi-category image segmentation which measures the ratio of intersection and concatenation of predicted pixels to real pixels in each category. MIoU takes into account the classification accuracy and coverage at the pixel level, and is able to evaluate the performance of the segmentation algorithm in a more comprehensive way.

The total accuracy provides a quick and intuitive evaluation of the overall performance of the algorithm, but it does not reflect well the differences in the segmentation performance of the algorithm in complex images or between different categories. In terms of accuracy, in some cases, we may be more interested in the classifier's prediction accuracy for positive examples, such as in target detection tasks. Precision rate measures how accurately a classifier recognizes a target region. In terms of recall, in other cases, we may be more interested in how well the classifier covers the target region, such as in semantic segmentation tasks. Recall measures whether the classifier recognizes all target regions. The equalization and concurrency ratio is a more appropriate evaluation metric in multi-category image segmentation tasks. It can take into account the classification accuracy and coverage at the pixel level to evaluate the performance of the segmentation algorithm in a more comprehensive way. Each of these metrics has its own focus, so when evaluating the performance of image segmentation algorithms, these metrics are usually considered in a comprehensive way to obtain more comprehensive evaluation results.

Table 3 provides an overview of the accuracy evaluation for each method employed in this study. Evaluated metrics include overall accuracy (OA), precision, recall, and Mean Intersection over Union (MIoU). The NDWI-Gumbel method demonstrated the highest overall accuracy at 91.75%, with precision, recall, and MIoU values of 92.21%, 91.87%, and 90.94%, respectively. These results underscore the robustness and effectiveness of the NDWI-Gumbel approach in accurately delineating water bodies. Other methods such as NDWI, NDWI-SVM, NDWI-K-means, and NDWI-GA also exhibited high overall accuracies ranging from 89.19% to 91.36%. However, slight variations were observed among these methods in terms of precision, recall, and MIoU. In contrast, the NDWI-MLE method showed slightly lower overall accuracy (84.43%) compared to other methods,

with correspondingly lower precision, recall, and MIoU values. This suggests that NDWI-MLE may be less effective in accurately identifying water bodies compared to the other evaluated methods. Overall, the results from Table 3 highlight that the NDWI-Gumbel method outperforms other methods in terms of overall accuracy and other evaluation metrics, making it the preferred choice for delineating water bodies in this study.

Table 3. Accuracy Evaluation Table for Each Method.

Method	OA	Precision	Recall	MIoU
NDWI-Gumbel	91.75%	92.21%	91.87%	90.94%
NDWI	91.36%	92.08%	92.23%	90.66%
NDWI-SVM	90.89%	91.32%	91.04%	90.04%
NDWI-Otsu	86.67%	87.11%	86.81%	85.49%
NDWI-K-means	89.61%	89.96%	89.37%	88.76%
NDWI-GA	89.19%	89.73%	89.45%	88.52%
NDWI-MLE	84.43%	85.04%	85.10%	83.71%
NDWI-Adaboost	87.26%	87.83%	87.14%	86.69%

4. Discussion

In this study, NDWI, a water body index, was used to extract information about the Qinghai Lake water body in 2023. The water body index method of extracting information about the water body is relatively simple and fast compared to machine learning and deep learning methods, but there are certain problems due to the similarity of spectral reflectance and absorption characteristics of some objects and the surface of the water body; the phenomenon of heterogeneous objects with the same spectrum exists; the glaciers around the study area and the snow also impinge into the water body; a small portion of shadows have also been misclassified as a water body; and repeated experiments to determine the optimal threshold by visual judgment are also more subjective. The method of determining the optimal threshold was also subjective.

The maximum interclass variance method is the Otsu method. This high efficiency, maximum interclass variance method (OTSU) is a fast and effective threshold selection method; the computational process is simple and fast, and it can effectively segment the image. The OTSU thresholding method obtains the optimal threshold by automatic calculation, which avoids errors due to a human-set threshold. There are also some shortcomings. Although the Otsu method can automatically select the threshold value, in practice, the selection of the threshold value may be affected by a variety of factors such as image quality, lighting conditions, etc., resulting in the threshold value between different images not being comparable. The extraction of information about large-scale water bodies may have the problem of omission or false alarm. Since the NDWI index is calculated based on image elements, the extraction of information about large-scale water bodies may not include recognition of the boundary of water bodies completely, resulting in false alarms or the omission of water bodies [4].

NDWI-SVM (Normalized Difference Water Index–Support Vector Machine) leverages the strengths of both NDWI and SVM, offering improved classification performance compared to NDWI alone. It provides a robust framework for accurately delineating water bodies across diverse landscapes. NDWI-SVM effectively addresses the limitations of NDWI by incorporating advanced classification techniques. It demonstrates high accuracy in differentiating water from other land cover types, even in complex environments. The SVM differs from Otsu’s method in that it does not require the traversing of all pixel values to compute and determine the segmentation threshold. Instead, it involves manually selecting specified pixel values corresponding to water and non-water regions, thereby informing the computer in advance about the segmentation criteria. These selected values are then fed into the model for training until it converges to an optimal or near-optimal solution. Subsequently, the entire image is inputted into the trained model to differentiate water and non-water regions, ultimately generating the segmented output. This approach is referred to as supervised classification. However, there are also limitations: NDWI-SVM may require careful parameter tuning and

extensive training data to optimize classification performance. It may also be computationally intensive, particularly for large-scale or high-resolution imagery [34].

The segmentation based on the Normalized Difference Water Index (NDWI) using the K-means method eliminates the need for pre-defined thresholds, distinguishing it from the Otsu and SVM approaches. K-means is an unsupervised clustering algorithm that autonomously clusters data according to its inherent structure, mitigating errors stemming from subjective threshold setting. This technique partitions data into multiple clusters, facilitating the discrimination between water bodies and other land cover types, thereby accurately extracting information about water bodies from intricate backgrounds. It boasts favorable visualization capabilities: K-means can visually represent data points in a two-dimensional space, aiding in comprehending data distribution and clustering outcomes [35]. Nonetheless, this method entails certain limitations. K-means is sensitive to the initial selection of cluster centers, whereby distinct initial centroids may yield divergent clustering results. In terms of vulnerability to noise and outliers, remote sensing imagery may contain noise and outliers, factors that may influence the clustering outcomes of K-means, resulting in errors in water body information extraction. Additionally, K-means exhibits high computational complexity, necessitating prolonged computation times for processing large-scale datasets.

Genetic algorithm (GA) is a global optimization search algorithm which transforms the problem-solving process into processes similar to the crossover and mutation of chromosome genes in biological evolution. Therefore, GA has many parameters, and among the eight methods described in this paper, it has the most parameters. Unlike supervised methods such as SVM and MLE, which preselect pixel values, GA has the longest computational segmentation time if pixel values are not manually selected. Adjusting the parameters will affect the convergence of the algorithm and may lead to misclassification and misjudgment. Some researchers have analyzed that when the mutation probability of GA is set to 0.3 and the crossover probability is set to 0.7, the convergence and performance of image segmentation problems can achieve relative optimization [36]. However, this finding should be taken with caution as it may not be directly applicable to image data, which are typically represented as uint8 values ranging from 0 to 255, while NDWI imagery is represented as decimal values ranging from -1 to 1. Therefore, this method is not recommended for practical applications and should be considered as a reference only.

Maximum likelihood estimation (MLE) classification is a statistical method that estimates unknown parameters based on the probability distribution of known samples. For water body information extraction from NDWI, this method can more accurately identify the boundaries and features of water bodies. Compared to other methods, it does not require the inputting of any parameters, nor does it require iterative parameter tuning or consideration of multiple factors. The only concern is the issue of sample purity, and the computational segmentation time is second only to GA and SVM.

AdaBoost is a water body information extraction method that combines multiple features and classifiers. Unlike the methods described previously, it does not aim to identify the most representative features of water bodies. Instead, it constructs simple classifiers using water body indices and combines them in a weighted manner through a “voting-based” approach. Each simple classifier conducts a “weighted vote” to achieve water body information extraction [37]. Due to its voting-based nature, majority voting determines the classification outcome, where the minority may be incorrectly classified, as illustrated in the segmentation image in the last row of Table 1. Furthermore, the AdaBoost algorithm encounters significant challenges in dealing with class imbalance issues. When the number of water body pixels greatly differs from non-water body pixels, it may affect the training process, leading to bias. Depending on parameter settings, it may tend to favor fewer or more instances.

The methodology proposed in this study extracts features based on the Normalized Difference Water Index (NDWI) and estimates the Gumbel parameter to determine the optimal threshold. It necessitates utilizing the pixel values of the entire NDWI image as input, with computational complexity rendering parallel processing unfeasible. Consequently,

the computational efficiency is significantly lower compared to that of the NDWI method. Moreover, due to calculations performed on NDWI, certain glaciers and snow can also be erroneously classified as water bodies.

Therefore, based on testing and analysis of various methods, it is advisable to select suitable approaches according to specific circumstances in practical applications. For instance, when dealing with large volumes of remote sensing imagery data, the NDWI-K-means method is recommended due to its simplicity and efficiency. Alternatively, for considerably larger datasets, employing methods such as NDWI-Gumbel or NDWI-SVM for water body extraction is suggested. However, segmentation results are suboptimal with NDWI-Otsu and NDWI-AdaBoost algorithms. Moreover, the NDWI-GA algorithm is not highly recommended due to its excessive parameterization.

In summary, each method offers unique strengths and limitations in water body detection, highlighting the importance of selecting an appropriate approach based on specific application requirements, image characteristics, and environmental conditions. Further research and comparative studies can provide valuable insights into the relative performance of these methods and guide their practical implementation in remote sensing applications.

From Figure 4, it can be seen that Qinghai Lake showed a turning point in 2004, with an overall decreasing trend before 2004, although there were drastic fluctuations. After 2004, it shows an upward trend, with a 6.9% increase in area over the 20-year period 2004–2023.

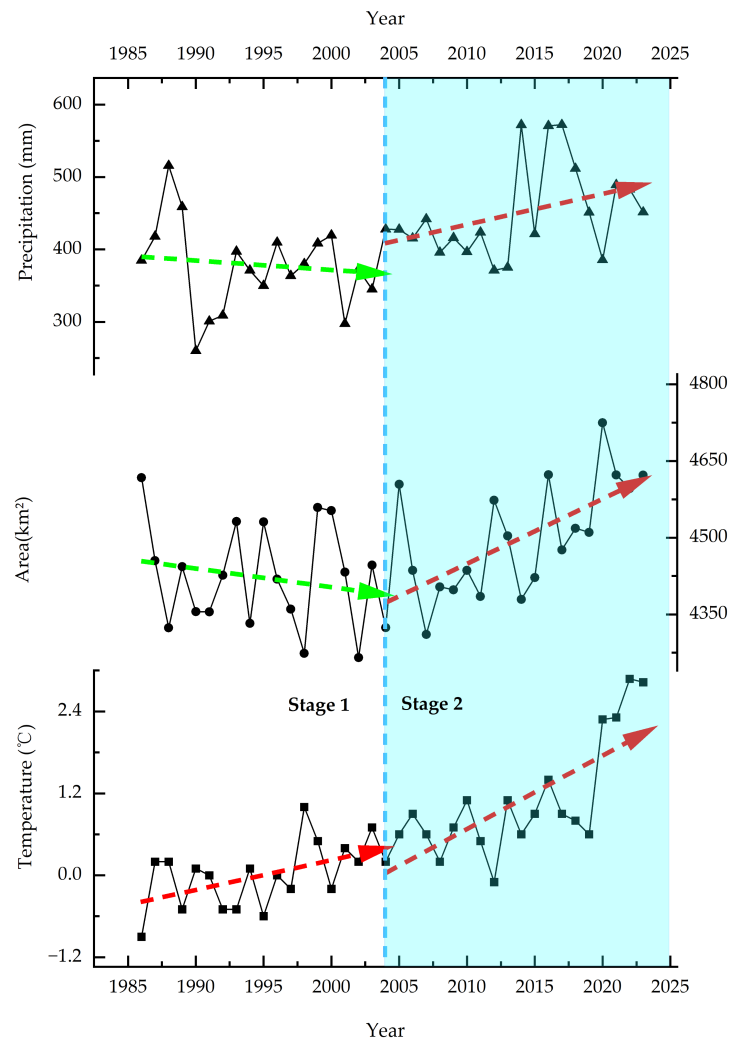


Figure 4. From top to bottom are the precipitation, area, and temperature data spanning 38 years for Qinghai Lake. Trend lines determined using the least squares method are depicted, with green arrows indicating a decline and red arrows indicating an increase. The data are divided into two stages, stage 1 and stage 2.

This is because the results of the study show that 93.13% of the water level changes can be attributed to climate change. In contrast, watershed changes accounted for only 6.87% [38]. This is a very important feature of global warming that has had far-reaching effects and influenced the hydrological changes in Qinghai Lake [39]. It is hypothesized to be due to climate warming.

To ascertain whether the expansion of Qinghai Lake's water body area is attributable to climate warming, we compiled and analyzed temperature and precipitation data spanning 38 years. As depicted in Figure 4, arranged from top to bottom are precipitation, area, and temperature. We delineated the data into two phases:

The first phase, predating 2004, was characterized by a gradual decline in precipitation and area alongside an ascending temperature trend. The second phase, from 2004 to the present, witnessed an upward trend in precipitation, area, and temperature. The trends illustrated in Figure 4 reveal that the area and temperature are increasing most rapidly, corroborating findings by Hongmei Dong et al. [30], wherein temperature rises annually by 0.13 degrees Celsius. According to the principle of water balance, water volume cannot spontaneously increase; therefore, the increased rate of glacier melt and the rapid degradation of permafrost, attributed to rising temperatures, account for the observed phenomena.

According to Hong Chen [40] and others, evapotranspiration and precipitation have low relevance and little effect on the water bodies of the Tibetan Plateau, while the most significant effect is on the temperature, and it was concluded that for every 1 °C increase in the temperature of the Tibetan Plateau, the area of the Tibetan Plateau's permanent water bodies increases by 0.291 million km², and the seasonal water bodies decrease by 0.001 million km².

The melting rate of alpine glaciers due to climate warming has greatly accelerated, changing the hydrological characteristics of the study area. According to the research, the alpine glacier reserve of 43,000 km² in northwest China is melting at an average rate of 243.7 km² per year [41]. In addition, the phenomenon of permafrost degradation has intensified, and during the past 40 years, from 1980 to 2019, the area of perennial permafrost on the Tibetan Plateau has decreased by 13.9%, and the underground ice reserves have decreased by about 401.1 Gt, which is about twice as much as the decrease in glacier reserves during the same period [42].

There is an island named Haixinyu in the center of Qinghai Lake which is 30 km away from the south shore, with an elevation of about 3300 m [43]. The land area of Haixinyu from 2003 to 2023 was extracted by Landsat remote sensing images using the method proposed in this paper; it is not large in size and the range of change is small. Due to the continuous expansion of the Qinghai Lake area, the water level rises, and the area of the Haixinyu decreases in the trend, as shown in Figure 5. With the continuous expansion of the water body area and the rise of the water level, the area of the Haixinyu of Qinghai Lake decreased by 14.07% in the last 20 years.

In this study, Pearson correlation coefficients were utilized to examine the relationship between temperature and lake area, as well as precipitation and lake area. Specifically, Figure 6 illustrates the outcomes of the correlation analysis, indicating a Pearson correlation coefficient of 0.2267 for temperature and lake area, and 0.39656 for precipitation and lake area. These Pearson correlation coefficients reflect the linear association between temperature and lake area, as well as precipitation and lake area. Specifically, the coefficient of 0.2267 falls within the range of 0 to 0.3, indicating a weak positive correlation between temperature and lake area, while the coefficient of 0.3966 signifies a moderate positive correlation between precipitation and lake area. This suggests that with increasing temperature, the area of Qinghai Lake may correspondingly expand.

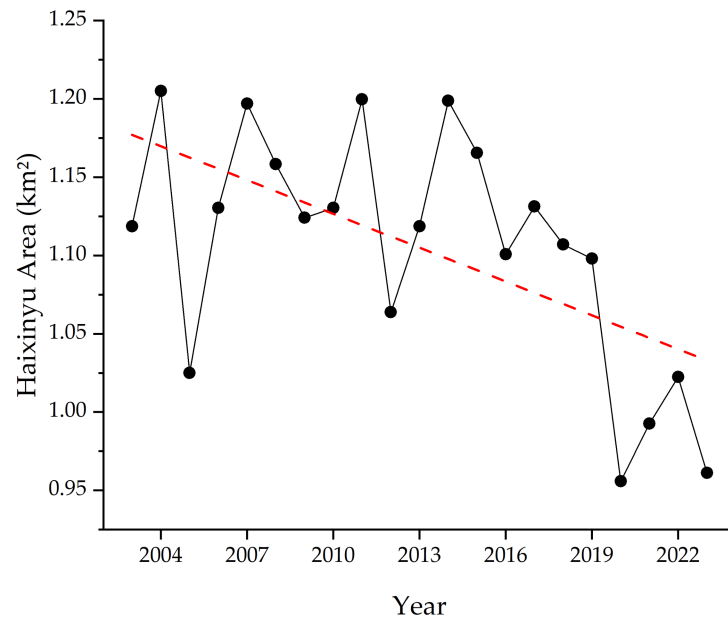


Figure 5. Trends in the area of Qinghai Lake’s Haixinyu, 2003–2023. The red dashed line in the above figure represents the trend line determined using least squares method.

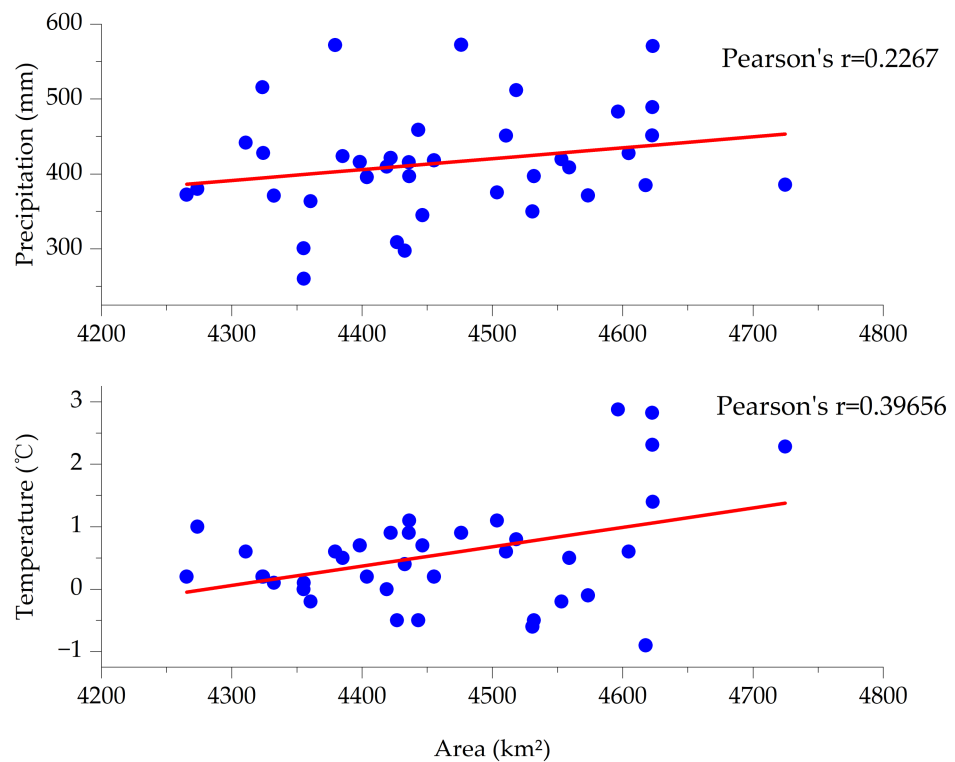


Figure 6. Area–precipitation and area–temperature correlation analysis graphs. The red dashed line in the above figure represents the trend line determined using least squares method.

Table 4 illustrates the Pearson correlation coefficients between two variables along with the results of their significance tests. The third column presents the *t*-values, which serve as statistical metrics for assessing the significance level of the correlation coefficients. In this table, the *t*-value for “area–temperature” is 2.5919, while for “area–precipitation” it is 1.3966. The fourth column displays the *p*-values, indicating the probability of observing the current *t*-value or a more extreme value under the null hypothesis. If the *p*-value is less than the designated significance level (typically 0.05), the null hypothesis can be rejected, suggesting

a significant correlation. In this context, the p -value for “area–temperature” is 0.0137, whereas for “area–precipitation” it is 0.1711. Overall, the correlation for “area–temperature” is significant at the 0.05 level of significance, while that for “area–precipitation” is not deemed significant.

Table 4. Pearson correlation coefficient significance test.

	r	t	p
Area–Temperature	0.3966	2.5919	0.0137
Area–Precipitation	0.2267	1.3966	0.1711

Under the influence of climate warming, the majority of the Tibetan Plateau experiences glacier melt and permafrost degradation. Glacial-fed lakes show an expanding trend. The continuous expansion of Qinghai Lake has resulted in the submergence of surrounding areas such as Tiebukabay, Quanwan, and Bird Island, including roads, docks, grasslands, and residential areas [44]. The fluctuation in the water level of Qinghai Lake causes the submergence of land animal feces and substances like nitrogen and phosphorus from the soil into the water, leading to a certain degree of eutrophication of Qinghai Lake, with the area of *Cladophora* algae blooms continuously increasing. According to the study by Duan H et al. [45], the maximum area of *Cladophora* algae blooms was 8.67 square kilometers in 2016; it then decreased in 2017, 2018, 2019, and 2020, with areas of 5.22 square kilometers, 3.32 square kilometers, 4.55 square kilometers, and 2.49 square kilometers, respectively. However, the maximum area reached 9.14 square kilometers in 2021. This may be attributed to the artificial harvesting efforts primarily conducted from 2017 to 2020, with another extensive outbreak of *Cladophora* algae blooms occurring in 2021 without any measures taken. This suggests that although artificial harvesting is an effective method, it cannot completely eradicate the issue.

5. Conclusions

In this study, based on Landsat 5/7/8/9 from 1986 to 2023, we analyzed the long-term change characteristics of Qinghai Lake’s area and verified the accuracy of the method proposed in this paper, based on the information extracted in the study area. Eight methods using NDWI-Gumbel, NDWI, NDWI-SVM, NDWI-Otsu, NDWI-K-means, NDWI-GA, NDWI-MLE, and NDWI-AdaBoost were used to compare the accuracy, and a total of 38 years of Qinghai Lake area data were extracted. It aims to comprehensively analyze the long-term area change in Qinghai Lake and provide data support and theoretical reference for the government and for other ecological and environmental studies of Qinghai Lake. The main conclusions are as follows:

1. The water body index method NDWI has the ability to suppress the vegetation, highlight the water body characteristics, and involves easy arithmetic. Based on the normalization operation of Landsat image green light band and near-infrared band, the great likelihood method is used to deduce the Gumbel parameter and establish the probability density expression so as to integrate and deduce the segmentation threshold T . Finally, based on the normalized water body index (NDWI), the genetic algorithm (GA), AdaBoost, the maximum interclass variance method (Otsu), the Support Vector Machine SVM, the maximum likelihood classification, clustering algorithm K-means, and this algorithm are used for accuracy comparison.
2. Based on the extraction of information about the area of Qinghai Lake for 38 years from 1986 to 2023 by the method proposed in this paper, the area of the water body of Qinghai Lake showed a decreasing trend during 1986–2004, and Qinghai Lake showed an expanding trend from 2004 to 2023, with an increase of 6.9% in the area during these 20 years.
3. There is an island named Haixinyu in the center of Qinghai Lake, with an area of about 1 km², and the method proposed in this paper extracts the island area of Haixinyu

during the 20 years from 2004 to 2023. Due to the expansion of the water body area of Qinghai Lake and the rise of the water level, the area of Haixinyu has been decreasing (it decreased to 0.9612 km² in 2023), and the area of Haixinyu in Qinghai Lake has decreased by 14.07% in the past 20 years.

4. According to the study, 93.13% of the water level changes can be attributed to climate change. The analysis of the causes of changes in Qinghai Lake includes climate warming (on the Tibetan Plateau, every 10 years the average temperature rose by 0.35°C), which has resulted in glacier melting and permafrost degradation intensifying. Glacier meltwater river area in the past ten years showed an increase in the trend. There are many factors influencing the change in lake area, such as temperature, precipitation, glacier, permafrost, etc., and different factors are interacting and transforming the water cycle. This study analyzes the influencing factors for selecting Qinghai Lake as the study area. The change is not comprehensive, and this study qualitatively analyzes the influencing factors of the change in the lake area of the Sanjiangyuan and cannot fully explain its reason.
5. We employed Pearson correlation analysis to reveal a moderate positive correlation between Qinghai Lake's area and temperature ($r = 0.3966$ and $p = 0.0137$, significant at the 0.05 level). This suggests that with increasing temperatures, there is a corresponding potential for expansion in Qinghai Lake's area. In contrast, the correlation between Qinghai Lake's area and precipitation showed no significant relationship ($r = 0.2267$ and $p = 0.1711$, not significant at the 0.05 level). These findings underscore the greater influence of temperature over precipitation in shaping the dynamics of Qinghai Lake's area. The observed potential for expansion with rising temperatures highlights the sensitivity of this ecosystem to climate change, particularly temperature fluctuations.

Author Contributions: Methodology, S.L.; Writing—review & editing, F.L.; Supervision, J.Q. All authors have read and agreed to the published version of the manuscript.

Funding: This research was funded by the National Natural Science Foundation of China under Grant Nos. 91847302, 51979276; the Key R&D program of the Science and Technology Department of Tibet under Grant No. XZ202101ZY0003G; OpenResearch Fund Program of State Key Laboratory of Hydrosience and Engineering under Grant No. sklhse-2021-B-06.

Data Availability Statement: The data from this study can be provided upon request by the corresponding author. Due to the need to patent the methods involved in the code, issues related to intellectual property design, and concerns regarding national security, the code and data are temporarily not available for public release.

Conflicts of Interest: The authors declare no conflict of interest.

References

1. Lu, J.; Qin, T.; Yan, D.; Lv, X.; Yuan, Z.; Wen, J.; Xu, S.; Yang, Y.; Feng, J.; Li, W. Response of Vegetation to Drought in the Source Region of the Yangtze and Yellow Rivers Based on Causal Analysis. *Remote Sens.* **2024**, *16*, 630. [[CrossRef](#)]
2. Zhao, L.; Zou, D.; Hu, G.; Du, E.; Pang, Q.; Xiao, Y.; Li, R.; Sheng, Y.; Wu, X.; Sun, Z.; et al. Changing climate and the permafrost environment on the Qinghai–Tibet (Xizang) plateau. *Permafr. Periglac. Process.* **2020**, *31*, 396–405. [[CrossRef](#)]
3. Work, E.A.; Gilmer, D.S. Utilization of satellite data for inventorying prairie ponds and lakes. *Photogramm. Eng. Remote Sens.* **1976**, *42*, 685–694.
4. Liu, S.; Wu, Y.; Zhang, G.; Lin, N.; Liu, Z. Comparing Water Indices for Landsat Data for Automated Surface Water Body Extraction under Complex Ground Background: A Case Study in Jilin Province. *Remote Sens.* **2023**, *15*, 1678. [[CrossRef](#)]
5. McFeeters, S.K. The use of the Normalized Difference Water Index (NDWI) in the delineation of open water features. *Int. J. Remote Sens.* **1996**, *17*, 1425–1432. [[CrossRef](#)]
6. Liu, J.; Jin, W.D. 3-dimensional adaptive minimum error threshold segmentation method. *Chin. Journal Image Graph.* **2013**, *18*, 1416–1424.
7. Nobuyuki, O. A threshold selection method from gray-level histograms. *IEEE Trans. Syst. Man Cybern.* **1979**, *9*, 62–66.
8. Kittler, J.; Illingworth, J. Minimum error thresholding. *Pattern Recognit.* **1986**, *19*, 41–47. [[CrossRef](#)]
9. Kapur, N.; Sahoo, P.K. A new method for gray-level picture thresholding using the entropy of the histogram. *Comput. Vis. Graph. Image Process* **1985**, *29*, 273–285. [[CrossRef](#)]
10. Cortes, C.; Vapnik, V. Support-vector network. *Mach. Learn.* **1995**, *20*, 273–297. [[CrossRef](#)]

11. Quinlan, R. Induction of decision trees. *Mach. Learn.* **1986**, *1*, 81–106. [[CrossRef](#)]
12. MacQueen, J. Some methods for classification and analysis of multivariate observations. *Proc. Fifth Berkeley Symp. Math. Stat. Probab.* **1967**, *1*, 281–297.
13. Goodfellow, I.; Bengio, Y.; Courville, A. *Deep Learning*; Zhao, S., Li, Y., Fu, T., Li, K., Eds.; People's Post and Telecommunications Publishing House: Beijing, China, 2022; p. 12.
14. Long, J.; Shelhamer, E.; Darrell, T. Fully convolutional networks for semantic segmentation. In Proceedings of the IEEE Conference on Computer Vision and Pattern Recognition, Boston, MA, USA, 7–12 June 2015; pp. 3431–3440.
15. Ulku, I.; Akagündüz, E. A survey on deep learning-based architectures for semantic segmentation on 2d images. *Appl. Artif. Intell.* **2022**, *36*, 2032924. [[CrossRef](#)]
16. Gao, Z.; Wang, A. Multi-scale image semantic segmentation based on ASPP and improved HRNet. *Chin. Ournal Liq. Cryst. Disp.* **2021**, *36*, 1497–1505.
17. Ronneberger, O.; Fischer, P.; Brox, T. U-net: Convolutional networks for biomedical image segmentation. In Proceedings of the Medical Image Computing and Computer-Assisted Intervention–MICCAI 2015: 18th International Conference, Munich, Germany, 5–9 October 2015; Proceedings, Part III 18. Springer International Publishing: Berlin/Heidelberg, Germany, 2015; pp. 234–241.
18. Wang, R.; Lei, T.; Cui, R.; Zhang, B.; Meng, H.; Nandi, A.K. Medical image segmentation using deep learning: A survey. *IET Image Process* **2022**, *16*, 1243–1267. [[CrossRef](#)]
19. Yu, F.; Koltun, V. Multi-scale context aggregation by dilated convolutions. *arXiv* **2015**, arXiv:1511.07122.
20. Chen, L.C.; Papandreou, G.; Kokkinos, I.; Murphy, K.; Yuille, A.L. Semantic image segmentation with deep convolutional nets and fully connected crfs. *arXiv* **2014**, arXiv:1412.7062.
21. Chen, L.C.; Papandreou, G.; Kokkinos, I.; Murphy, K.; Yuille, A.L. Deeplab: Semantic image segmentation with deep convolutional nets, atrous convolution, and fully connected crfs. *IEEE Trans. Pattern Anal. Mach. Intell.* **2017**, *40*, 834–848. [[CrossRef](#)]
22. Chen, L.C.; Papandreou, G.; Schroff, F.; Adam, H. Rethinking atrous convolution for semantic image segmentation. *arXiv* **2017**, arXiv:1706.055872.
23. Chen, L.C.; Zhu, Y.; Papandreou, G.; Schroff, F.; Adam, H. Encoder-decoder with atrous separable convolution for semantic image segmentation. In Proceedings of the European Conference on Computer Vision (ECCV), Munich, Germany, 8–14 September 2018; pp. 801–818.
24. He, K.; Zhang, X.; Ren, S.; Sun, J. Deep residual learning for image recognition. In Proceedings of the IEEE Conference on Computer Vision and Pattern Recognition, Las Vegas, NV, USA, 27–30 June 2016; pp. 770–778.
25. Huang, G.; Liu, Z.; Van Der Maaten, L.; Weinberger, K.Q. Densely connected convolutional networks. In Proceedings of the IEEE Conference on Computer Vision and Pattern Recognition, Honolulu, HI, USA, 21–26 July 2017.
26. Sun, K.; Xiao, B.; Liu, D.; Wang, J. Deep high-resolution representation learning for human pose estimation. In Proceedings of the IEEE Conference on Computer Vision and Pattern Recognition, Long Beach, CA, USA, 15–20 June 2019; pp. 5693–5703.
27. Baidu Online Encyclopedia—Gumbel Distribution [EB/OL]. 2023. Available online: https://baike.baidu.com/item/%E8%80%BF%E8%B4%9D%E5%B0%94%E5%88%86%E5%B8%83/1381013?fr=ge_ala (accessed on 12 December 2023).
28. Bhanu, B.; Lee, S.; Ming, J. Adaptive image segmentation using a genetic algorithm. *IEEE Trans. Syst. Man Cybern.* **1995**, *25*, 1543–1567. [[CrossRef](#)]
29. Lupascu, C.A.; Tegolo, D.; Trucco, E. FABC: Retinal vessel segmentation using AdaBoost. *IEEE Trans. Inf. Technol. Biomed.* **2010**, *14*, 1267–1274. [[CrossRef](#)] [[PubMed](#)]
30. Dong, H.; Song, Y.; Zhang, M. Hydrological trend of Qinghai Lake over the last 60 years: Driven by climate variations or human activities? *J. Water Clim. Chang.* **2019**, *10*, 524–534. [[CrossRef](#)]
31. Tucker, C.; Sellers, P. Satellite remote sensing of primary production. *Int. J. Remote Sens.* **1986**, *7*, 1395–1416. [[CrossRef](#)]
32. Huang, S.; Jiang, W.; Zhou, T.; Sun, H. Remote sensing of Extracting Water Depth based on Support Vector Machine. In Proceedings of the 2011 International Conference on Future Computer Science and Education, Xi'an, China, 20–21 August 2011; pp. 369–372.
33. Wang, W.; Teng, H.; Zhao, L.; Han, L. Long-Term Changes in Water Body Area Dynamic and Driving Factors in the Middle-Lower Yangtze Plain Based on Multi-Source Remote Sensing Data. *Remote Sens.* **2023**, *15*, 1816. [[CrossRef](#)]
34. Özelkan, E. Comparison of remote sensing classification techniques for water body detection: A case study in Atikhisar Dam Lake (Çanakkale). *Cumhur. Sci. J.* **2019**, *40*, 650–661. [[CrossRef](#)]
35. Dhanachandra, N.; Manglem, K.; Chanu, Y. Image segmentation using K-means clustering algorithm and subtractive clustering algorithm. *Procedia Comput. Sci.* **2015**, *54*, 764–771. [[CrossRef](#)]
36. Kalkreuth, R.; Rudolph, G.; Krone, J. Improving convergence in cartesian genetic programming using adaptive crossover, mutation and selection. In Proceedings of the 2015 IEEE Symposium Series on Computational Intelligence, Cape Town, South Africa, 7–10 December 2015; pp. 1415–1422.
37. Shen, L.; Li, C. Water body extraction from Landsat ETM+ imagery using adaboost algorithm. In Proceedings of the 2010 18th International Conference on Geoinformatics, Beijing, China, 18–20 June 2010; pp. 1–4.
38. Fang, J.; Li, G.; Rubinato, M.; Ma, G.; Zhou, J.; Jia, G.; Yu, X.; Wang, H. Analysis of long-term water level variations in Qinghai Lake in China. *Water* **2019**, *11*, 2136. [[CrossRef](#)]
39. Ji, S.; Xingqi, L.; Sumin, W.; Matsumoto, R. Palaeoclimatic changes in the Qinghai Lake area during the last 18,000 years. *Quat. Int.* **2005**, *136*, 131–140. [[CrossRef](#)]

40. Hong, C.; Wang, M.; Zhu, F. Terrain-sensitive water body extraction and its application to the Tibetan Plateau. *Geospat. Inf.* **2022**, *20*, 43–47.
41. Cold and Arid Regions Environmental and Engineering Research Institute, Chinese Academy of Sciences. *Second Inventory of Glaciers in China*; Chinese Academy of Science: Beijing, China, 2015.
42. Wang, T.; Yang, D.; Yang, Y.; Zheng, G.; Jin, H.; Li, X.; Yao, T.; Cheng, G. Unsustainable water supply from thawing permafrost on the Tibetan Plateau in a changing climate. *Sci. Bull.* **2023**, *68*, 1105–1108. [[CrossRef](#)] [[PubMed](#)]
43. Xinsha, H.; Climate Investigation Group. Climate Investigation of Haixin Mountain, Qinghai Lake. *Meteorology* **1985**, 23–25. Available online: https://kns.cnki.net/kcms2/article/abstract?v=n93avYlexq8eIX6LSmyoFCbuxcR1cF-PdJwIFIfD6vE1jtHOB6oPlzXyJzN2yazSQBuBCI6YaE2vo_AcuuIplwXZ2j0rFZTyCy3n07YYurnnGT0a4GkyxPeX1d2uaaZ_hS_VIxeikn0=&uniplatform=NZKPT&language=CHS (accessed on 12 December 2023).
44. Liang, B.; Qi, S.; Li, Z.; Li, Y.; Chen, J. Dynamic change of Lake Qinghai shoreline from 1973 to 2018. *Lake Sci.* **2020**, *32*, 573–586.
45. Duan, H.; Yao, X.; Zhang, D.; Jin, H.; Wei, Q. Long-term temporal and spatial monitoring of cladophora blooms in qinghai lake based on multi-source remote sensing images. *Remote Sens.* **2022**, *14*, 853. [[CrossRef](#)]

Disclaimer/Publisher’s Note: The statements, opinions and data contained in all publications are solely those of the individual author(s) and contributor(s) and not of MDPI and/or the editor(s). MDPI and/or the editor(s) disclaim responsibility for any injury to people or property resulting from any ideas, methods, instructions or products referred to in the content.